

# Stochastic resonance with a single metastable state: Thermal instability in NbN superconducting stripline resonators

Eran Segev,\* Baleegh Abdo, Oleg Shtempluck, and Eyal Buks  
 Department of Electrical Engineering, Technion, Haifa 32000, Israel

(Received 2 August 2007; revised manuscript received 18 October 2007; published 14 January 2008)

We study thermal instability in NbN superconducting stripline resonators. The system exhibits extreme nonlinearity near a bifurcation, which separates a monostable zone and an astable one. The lifetime of the metastable state, which is locally stable in the monostable zone, is measured near the bifurcation and the results are compared with a theory. Near bifurcation, where the lifetime becomes relatively short, the system exhibits strong amplification of a weak input modulation signal. We find that the frequency bandwidth of this amplification mechanism is limited by the rate of thermal relaxation. When the frequency of the input modulation signal becomes comparable or larger than this rate, the response of the system exhibits subharmonics of various orders.

DOI: [10.1103/PhysRevB.77.012501](https://doi.org/10.1103/PhysRevB.77.012501)

PACS number(s): 74.40.+k, 02.50.Ey, 85.25.-j

Stochastic resonance (SR) is a phenomenon in which metastability in nonlinear systems is exploited to achieve amplification of weak signals.<sup>1-3</sup> SR has been experimentally demonstrated in electrical, optical, superconducting, neuronal, and mechanical systems.<sup>4-12</sup> Usually, SR is achieved by operating the system in a region in which it has two metastable states and its response exhibits hysteresis. Under some appropriate conditions, a weak input signal, which modulates the transition rates between these states, can lead to synchronized noise-induced transitions, thus allowing strong amplification.

In this Brief Report, we investigate SR and amplification in a superconducting (SC) NbN stripline resonator. Contrary to previous studies, we operate the system near a bifurcation between a monostable zone, in which the system has a single metastable state, and an astable zone, in which this state ceases to exist and the system lacks any steady states. In our previous studies, we have investigated several effects, e.g., strong amplification,<sup>13</sup> noise squeezing,<sup>13</sup> and response to optical illumination,<sup>14,15</sup> which occur near this bifurcation, and limit cycle oscillations, which are observed in the astable zone.<sup>16,17</sup> In the present work, we investigate experimentally and theoretically the response of the system to an amplitude modulated input signal and find an unusual SR mechanism that has both properties of extremely strong responsivity and nonhysteretic behavior. The frequency bandwidth of this mechanism is found to be limited by the rate of thermal relaxation. We find that rather unique subharmonics of various orders are generated when the modulation frequency becomes comparable or larger than the relaxation rate. Moreover, we measure the lifetime of the metastable state in the monostable zone near the bifurcation and compare the results with a theory.

Our experiments are performed using a device that integrates a narrow microbridge into a SC stripline electromagnetic resonator. Design considerations, fabrication details, as well as resonance modes calculation can be found elsewhere.<sup>14</sup> The dynamics of our system can be captured by two coupled equations of motion, which are hereby briefly described (see Ref. 17 for a detailed derivation). Consider a resonator driven by a weakly coupled feed line

carrying an incident amplitude modulated coherent tone  $b^{\text{in}} = b_0^{\text{in}} \{1 + a \cos(\omega_m t)\} e^{-i\omega_p t}$ , where  $b_0^{\text{in}}$  is a constant complex amplitude,  $\omega_p = 2\pi f_p$  is the driving angular frequency,  $a$  is the modulation depth, and  $\omega_m = 2\pi f_m$  ( $\ll \omega_p$ ) is the angular modulation frequency. The mode amplitude inside the resonator can be written as  $B e^{-i\omega_p t}$ , where  $B(t)$  is a complex amplitude, which is assumed to vary slowly on a time scale of  $1/\omega_p$ . In this approximation, the equation of motion of  $B$  reads<sup>18</sup>

$$\frac{dB}{dt} = [i(\omega_p - \omega_0) - \gamma]B - i\sqrt{2}\gamma_1 b^{\text{in}} + F_n, \quad (1)$$

where  $\omega_0 = 2\pi f_0$  is the angular resonance frequency and  $\gamma = \gamma_1 + \gamma_2$ , where  $\gamma_1$  is the coupling coefficient between the resonator and the feed line and  $\gamma_2$  is the damping rate of the mode. The term  $F_n$  represents an input noise with a random phase  $\langle F_n(t) \rangle = 0$  and an autocorrelation function which, for relatively high temperature  $k_B T_{\text{eff}} \gg \hbar \omega_0$ , is given by<sup>18</sup>

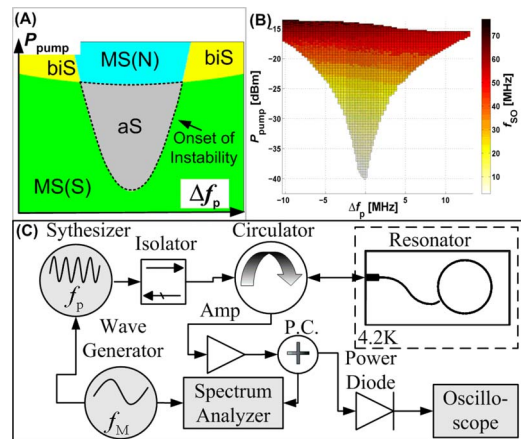


FIG. 1. (Color online) (a) System stability diagram and (b) self-oscillation frequency  $f_{\text{SO}}$  plotted as a function of the injected pump power  $P_{\text{pump}}$  and frequency detuning  $\Delta f_p = f_p - f_0$ , where  $f_p$  is the pump frequency and  $f_0$  is the resonance frequency. (C) Experimental setup.

$$\langle F_n^*(t')F_n(t) \rangle = 2\gamma \frac{k_B T_{\text{eff}}}{\hbar \omega_0} \delta(t' - t), \quad (2)$$

where the effective noise temperature is given by

$$T_{\text{eff}} = \frac{\gamma_1 T_n + \gamma_2 T_0}{\gamma}, \quad (3)$$

$T_n$  is the effective temperature of the feed line, and  $T_0$  is the temperature of the coolant.

The microbridge heat balance equation reads<sup>16</sup>

$$C \frac{dT}{dt} = 2\hbar \omega_0 \gamma_2 |B|^2 - H(T - T_0), \quad (4)$$

where  $T$  is the temperature of the microbridge,  $C$  is the thermal heat capacity, and  $H$  is the heat transfer coefficient.

Coupling between Eqs. (1) and (4) originates by the dependence of the damping rate  $\gamma_2(T)$  of the driven mode on the resistance of the microbridge,<sup>19</sup> which, in turn, depends on its temperature. We assume the simplest case where this dependence is a step function that occurs at the critical temperature  $T_c \approx 10$  K of the superconductor, namely,  $\gamma_2$  takes the value  $\gamma_{2s}$  for the SC phase ( $T < T_c$ ) of the microbridge and  $\gamma_{2n}$  for the normal-conducting (NC) phase ( $T > T_c$ ).

Solutions of steady state response to a monochromatic excitation (no modulation  $a=0$ ) are found by seeking stationary solutions to Eqs. (1) and (4) for the noiseless case  $F_n=0$ . Due to the coupling, the system may have, in general, up to two metastable states, corresponding to the SC and NC phases of the microbridge. The stability of each of these phases depends on both the power,  $P_{\text{pump}} \propto |b^{\text{in}}|^2$ , and frequency detuning  $\Delta f_p = f_p - f_0$  parameters of the injected pump tone. Our system has four stability zones [Fig. 1(a)].<sup>17</sup> Two are monostable zones [MS(S) and MS(N)], where either the SC or the NC phases are locally stable, respectively. Another is a bistable zone (BiS), where both phases are locally stable.<sup>20,21</sup> The third is an astable zone (aS), where none of the phases are locally stable. When the resonator is biased to the astable zone, the microbridge self-oscillates between the SC and NC phases.<sup>16,17</sup> The frequency of these self-oscillations is shown in Fig. 1(b) as a function of the exiting pump power and frequency  $\Delta f_p$ , where  $\Delta f_p = f_p - f_0$  and  $f_0 = 4.363$  GHz. Further experimental and numerical study of the self-oscillation phenomenon in the astable zone can be found in Refs. 16 and 17. The onset of this instability, namely, the bifurcation threshold (BT), is defined as the boundary of the astable zone [see Fig. 1(a)].

The experimental setup is depicted in Fig. 1(c). All experiments were done while the device was fully immersed in liquid helium. We inject an amplitude modulated pump tone into the resonator and measure the reflected power in the frequency domain using a spectrum analyzer and in the time domain using an oscilloscope. The parameters used for the numerical simulation were obtained as follows. The coupling coefficient  $\gamma_1 = 2$  MHz and the damping rates  $\gamma_{2s} = 2.2$  MHz,  $\gamma_{2n} = 64$  MHz were extracted from a frequency response measurement,<sup>14,20</sup> whereas the thermal heat capacity  $C$

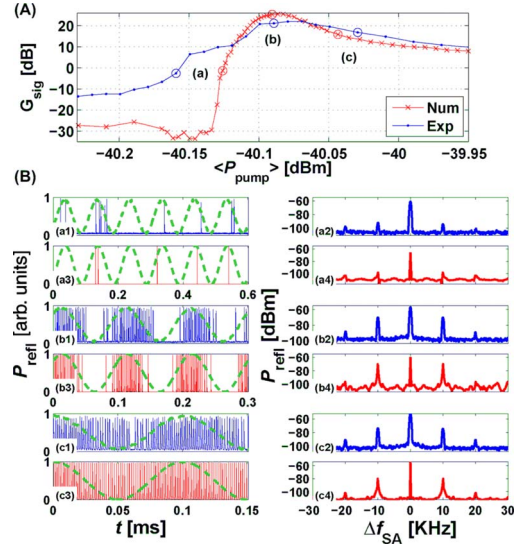


FIG. 2. (Color online) (A) Experimental (dotted, blue) and numerical (crossed, red) results of the signal amplification  $G_{\text{sig}}$  as a function of the mean injected pump power  $\langle P_{\text{pump}} \rangle$ . (B) Experimental [subplots (x1) and (x2)] and numerical [subplots (x3) and (x4)] results of the reflected power  $P_{\text{refl}}$  as a function of time [subplots (x1) and (x3)] and scanned frequency  $f_{\text{SA}}$  [subplots (x2) and (x4)], centered on the resonance frequency  $f_0$  ( $\Delta f_{\text{SA}} = f_{\text{SA}} - f_0$ ), where  $x$  denotes  $a$ ,  $b$ , and  $c$ , corresponding to the marked points in panel (A). The dashed (green) curve represents the modulation signal. The time domain measurements are normalized by their maximum peak to peak value.

$= 54 \text{ nJ cm}^{-2} \text{ K}^{-1}$  and the heat transfer coefficient  $H = 12 \text{ W cm}^{-2} \text{ K}^{-1}$  were calculated analytically according to Refs. 22 and 23.

Our system exhibits an extremely strong amplification when tuned to the BT. Figure 2 shows both experimental [subplots (x1) and (x2)] and numerical [subplots (x3) and (x4)] results for the case where the system is driven by a modulated pump tone tuned to the resonance frequency,  $f_p = f_0$ , and having the following modulation parameters:  $f_m = 10$  kHz and  $a = 0.0024$ . The numerical calculation assumes noise temperature of  $T_n = 75$  K in order to account for the influence of the phase noise of the synthesizer. Panel (A) in Fig. 2 plots the signal gain  $G_{\text{sig}}$ , defined as the ratio between the reflected power at frequency  $f_p + f_m$  and the sum of the injected powers at frequencies  $f_p \pm f_m$ , as a function of the mean injected pump power  $\langle P_{\text{pump}} \rangle$ , swept across the power threshold  $P_c$ , which separates the MS(S) and aS zones ( $P_c \approx -40.08$  dBm for  $f_p = f_0$ ). The system exhibits large gain of approximately 20 dB around the BT. The experimental results exhibit excess gain below BT relative to the numerical results. This can be explained by additional nonlinear mechanisms<sup>24</sup> that may induce small amplification and are not theoretically included in our piecewise linear model.

Figure 2(b) shows time and frequency domain results of the reflected power for three pairs of input power values ( $P_{\text{pump}}^{(a)} = -40.16$  dBm,  $P_{\text{pump}}^{(b)} = -40.09$  dBm, and  $P_{\text{pump}}^{(c)} = -40.02$  dBm), corresponding to the marked points [(a)–(c)] in panel (A). In addition, the time domain measurements contain a green-dashed curve showing the modulating signal.

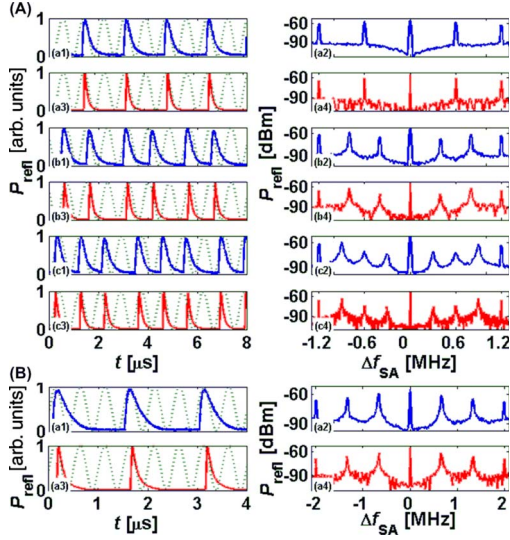


FIG. 3. (Color online) Experimental [subplots (x1) and (x2)] and numerical [subplots (x3) and (x4)] results showing subharmonic generation for the case of (A)  $f_m=1.2$  MHz and (B)  $f_m=2$  MHz. The reflected power  $P_{\text{refl}}$  is plotted as a function of time [subplots (x1) and (x3)] and scanned frequency  $f_{\text{SA}}$  [subplots (x2) and (x4)], centered on the resonance frequency  $f_0$  ( $\Delta f_{\text{SA}}=f_{\text{SA}}-f_0$ ), where  $x$  denotes  $a$ ,  $b$ , and  $c$ . Subplots (a)–(c) of panel (A) show subharmonics of the second, third, and fourth orders, respectively. Panel (B) shows subharmonics of the third order. The dashed (green) curve represents the modulation signal. The time domain measurements are normalized by their maximum peak to peak value.

The results shown in subplots (a1)–(a4) were obtained while biasing the system below the BT ( $\langle P_{\text{pump}} \rangle < P_c$ ). In general, the spikes in the time domain plots of Fig. 2(b) indicate events in which the temperature  $T$  temporarily exceeds  $T_c$ .<sup>17</sup> Below threshold, the average time between such events, which are induced by input noise, is the lifetime  $\Gamma^{-1}$  of the metastable state of the resonator. As we will show in the last part of this Brief Report,  $\Gamma$  strongly depends on the pump power near BT; thus, power modulation results in a modulation of the rate of spikes, as can be seen both in the experimental and simulation results.

Subplots (b1)–(b4) in Fig. 2(b) show experiments in which  $\langle P_{\text{pump}} \rangle \approx P_c$ , and thus the modulation itself drives the resonator in and out the astable zone. As a result, during approximately half of the modulation period, nearly regular spikes in reflected power are observed, whereas during the other half, only few noise-induced spikes are triggered. This behavior leads to a very strong gain as well as to the creation of higher order frequency components [subplots (b2) and

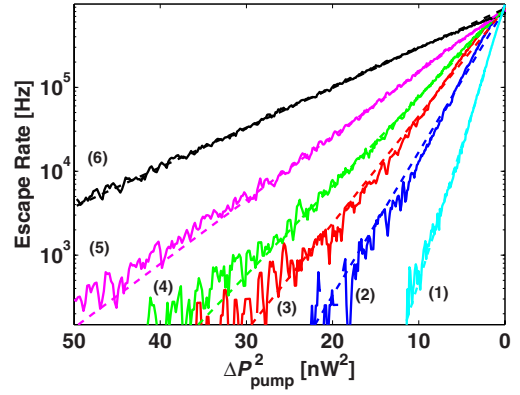


FIG. 4. (Color online) Escape rate. The solid curves show experimental data, and the dashed curves show the corresponding theoretical fit. The escape rate is shown for six different values of injected noise temperatures  $T_n$ , which are given by Table I.

(b4)]. Subplots (c1)–(c4) in Fig. 2(b) show experiments in which  $\langle P_{\text{pump}} \rangle > P_c$ , and thus the regular spikes occur throughout the modulation period. The rate of the spikes is strongly correlated to the injected power<sup>16</sup> and is higher for stronger pump powers [see Fig. 1(b)]. Therefore, the modulation of the pump power modulates, in turn, the rate of the spikes. This behavior also creates a rather strong amplification, though weaker than the one achieved in the previous case.

Each spike in subplots (a1) and (a2) of Fig. 2(b) lasts approximately  $1 \mu\text{s}$ , after which the device is ready to detect a new event. This recovery time determines the detection bandwidth. A measurement of the dependence of the amplification mechanism on the modulation frequency  $f_m$  has revealed a mechanism in which subharmonics of the modulation frequency are generated by the device. The generation of the subharmonics occurs when the modulation period is comparable to the recovery time of the system. The results are shown in Fig. 3, which shows both experimental [subplots (x1) and (x2)] and numerical [subplots (x3) and (x4)] results for the case of  $f_p=f_0$ ,  $a=0.017$ ,  $T_n=75$  K, and  $f_m=1.2$  MHz for panel (A) and  $f_m=2$  MHz for panel (B). Subplots (a)–(c) of panel (A) show the reflected power, obtained for three gradually increased pump power values ( $P_{\text{pump}}^{(a)}=-40.2$  dBm,  $P_{\text{pump}}^{(b)}=-40.07$  dBm, and  $P_{\text{pump}}^{(c)}=-40.0$  dBm) and corresponding to subharmonic generation (SHRG) of the second, third, and fourth orders. SHRG of the third order, for example, is generated by a quasiperiodic response of the system [subplots (a1) and (a3)]. Each quasiperiod lasts three modulation cycles, where only during the first two a spike occurs, namely, a spike is absent once every three modulation cycles. This behavior originates from the mismatch be-

TABLE I. Escape rate parameters.  $T_n$  is the measured noise temperature and  $P_c$  is the numerically fitted critical pump power.

	1	2	3	4	5	6
Measured $T_n$ ( $10^5$ K)	0.52	1	1.36	1.64	2.3	3.76
Fitted $P_c$ (nW)	125.1	121.6	120.4	119.9	118.9	117.2

tween the modulation period and the recovery time of a spike, which induces a phase difference that is monotonically accumulated, between the two. Once every  $n=3$  modulation cycles, in this case, the system fails to achieve critical conditions near the time where the peak in the modulation occurs, and therefore a spike is not triggered. Similar behavior is also shown in subplots (a1) and (a3) and subplots (c1) and (c3), where the quasiperiod lasts two and four modulation cycles, respectively.

Another mechanism for SHRG is observed when the modulation frequency is increased. Figure 3(b) shows measurement results for  $f_m=2$  MHz and  $P_{\text{pump}}=-40.05$  dBm, which demonstrate SHRG of order  $n=3$ . Unlike the previous case, this SHRG is characterized by a single spike that occurs once every three modulation cycles.

The fluctuation-induced escape rate  $\Gamma$  of the metastable state, which is locally stable in the MS(S) zone, strongly depends on the pump power near the BT. Consequently, the amplitude modulation of the injected pump tone results in a strong modulation in  $\Gamma$ . As we have demonstrated above, this mechanism can be exploited for small signal amplification by tuning the system into SR. In Ref. 25, we have found theoretically that

$$\Gamma = \Gamma_0 \exp\left(-\frac{\gamma_1 \Delta P_{\text{pump}}^2}{2\gamma_2^2 k_B T_{\text{eff}} P_{\text{pump}}}\right), \quad (5)$$

where  $\Gamma_0 = \sqrt{H\gamma/C}/2\pi$  and the power difference is given by  $\Delta P_{\text{pump}} \equiv P_c - P_{\text{pump}}$ . Note that the unusual scaling law in the present case  $\log(\Gamma/\Gamma_0) \propto \Delta P_{\text{pump}}^2$ , which differs from the commonly obtained scaling law of  $\log(\Gamma/\Gamma_0) \propto \Delta P_{\text{pump}}^{3/2}$ ,<sup>26,27</sup> is a signature of the piecewise linear dynamics of our system. Note also that in our case,  $\gamma_1$  is of the order of  $\gamma_2$  and  $T_n \gg T_0$  ( $T_0=4.2$  K); thus, the base temperature has a negligible effect on the effective temperature, namely,  $T_{\text{eff}} \approx T_n$ .

The escape rate was experimentally measured for several levels of injected noise temperatures  $T_n$ , which are given by Table I. In this experiment, we externally combine the usual amplitude modulated pump tone, which is tuned to the reso-

nance frequency  $f_p=f_0$  and slightly below the power threshold together with white noise generated by a broadband white noise source. The combined signal is injected into the resonator, and the reflected power is measured in the time domain. The modulation frequency was set to 500 Hz, which is more than 3 orders of magnitude lower than the relaxation rate of the system, and therefore to a good approximation the system follows this modulation adiabatically.<sup>26</sup>

The results are shown in Fig. 4, which plots the escape rate in logarithmic scale as a function of  $\Delta P_{\text{pump}}^2$ . Six pairs of solid and dashed curves are shown, corresponding to the six different levels of injected noise intensities. The solid curves were extracted from time domain measurements of the reflected power. The dashed curves were obtained by numerically fitting the experimental data to Eq. (5) and show good quantitative agreement between the experimental results and Eq. (5). The fitting parameters included the prefactor  $\Gamma_0 = 0.86$  MHz that was determined by a separate fitting process and  $P_c$  (see Table I) that slightly decreases with the increasing thermal noise. This behavior can be explained by local heating of the microbridge, induced by the noise that is injected into the resonator through other resonance modes. Note that  $T_n$  was extracted from a direct measurement of the injected noise intensity (see Table I). Note also that the system recovery time imposes an upper limit upon the measured escape rate. Thus, the escape rate close to the threshold might be higher than measured.

In summary, a mechanism of SR with a single metastable state has been demonstrated. Near BT, the system exhibits rich dynamical effects including bifurcation amplification and SHRG. In spite of its simplicity, our theoretical model successfully accounts for most of the experimental results.

We thank Steve Shaw and Mark Dykman for valuable discussions and helpful comments. This work was supported by the German Israel Foundation under Grant No. 1-2038.1114.07, the Israel Science Foundation under Grant No. 1380021, the Deborah Foundation, the Poznanski Foundation, Russel Berrie Nanotechnology Institute, and MAFAT.

\*segeve@tx.technion.ac.il

<sup>1</sup>R. Benzi *et al.*, SIAM J. Appl. Math. **43**, 565 (1983).  
<sup>2</sup>L. Gammaitoni *et al.*, Rev. Mod. Phys. **70**, 223 (1998).  
<sup>3</sup>T. Wellens *et al.*, Rep. Prog. Phys. **67**, 45 (2004).  
<sup>4</sup>S. Fauve and F. Heslot, Phys. Lett. **97**, 5 (1983).  
<sup>5</sup>B. McNamara *et al.*, Phys. Rev. Lett. **60**, 2626 (1988).  
<sup>6</sup>R. Rouse *et al.*, Phys. Rev. Lett. **75**, 1614 (1995).  
<sup>7</sup>A. D. Hibbs *et al.*, J. Appl. Phys. **77**, 2582 (1995).  
<sup>8</sup>B. Abdo *et al.*, Phys. Lett. A **370**, 449 (2007).  
<sup>9</sup>A. Longtin *et al.*, Phys. Rev. Lett. **67**, 656 (1991).  
<sup>10</sup>J. E. Levin and J. P. Miller, Nature (London) **380**, 165 (1996).  
<sup>11</sup>R. L. Badzey and P. Mohanty, Nature (London) **437**, 995 (2005).  
<sup>12</sup>C. Stambaugh and H. B. Chan, Phys. Rev. B **73**, 172302 (2006).  
<sup>13</sup>E. Segev *et al.*, Phys. Lett. A **366**, 160 (2007).  
<sup>14</sup>E. Arbel-Segev *et al.*, IEEE Trans. Appl. Supercond. **16**, 1943

(2006).

<sup>15</sup>E. Segev *et al.*, Phys. Lett. A **370**, 202 (2007).  
<sup>16</sup>E. Segev *et al.*, Europhys. Lett. **78**, 57002 (2007).  
<sup>17</sup>E. Segev *et al.*, J. Phys.: Condens. Matter **19**, 096206 (2007).  
<sup>18</sup>B. Yurke and E. Buks, J. Lightwave Technol. **24**, 5054 (2006).  
<sup>19</sup>D. Saeedkia *et al.*, IEEE Microw. Wirel. Compon. Lett. **15**, 510 (2005).  
<sup>20</sup>B. Abdo *et al.*, IEEE Trans. Appl. Supercond. **16**, 1976 (2006).  
<sup>21</sup>B. Abdo *et al.*, Phys. Rev. B **73**, 134513 (2006).  
<sup>22</sup>M. W. Johnson *et al.*, J. Appl. Phys. **79**, 7069 (1996).  
<sup>23</sup>K. Weiser *et al.*, J. Appl. Phys. **52**, 4888 (1981).  
<sup>24</sup>M. A. Golosovsky *et al.*, Phys. Rev. B **51**, 6462 (1995).  
<sup>25</sup>B. Abdo *et al.*, J. Appl. Phys. **101**, 083909 (2007).  
<sup>26</sup>M. I. Dykman *et al.*, Phys. Rev. Lett. **92**, 080602 (2004).  
<sup>27</sup>M. Bier, Phys. Rev. E **71**, 011108 (2005).